TITLE:

Experimental investigation on the flow structure over a delta wing via flow visualization methods

AUTHORS & AFFILIATIONS:

Lu Shen[1], Zong-nan Chen[1] & Chih-yung Wen[1,*]

[1]*Department of Mechanical Engineering, The Hong Kong Polytechnic University, Hong Kong*

**Corresponding Author:* Chih-yung Wen

Email Address: cywen@polyu.edu.hk

Tel: +852-27666644

KEYWORDS:

Delta wing; smoke flow visualization; leading edge vortex; vortex breakdown; vortex oscillation; particle image velocimetry

SHORT ABSTRACT:

Here, we present a protocol to observe unsteady vortical flows over a delta wing using a modified smoke flow visualization technique and investigate the mechanism responsible for the oscillations of the leading edge vortex breakdown locations.

LONG ABSTRACT:

It is well known that the flow field over a delta wing is dominant by a pair of counter rotating leading edge vortices (LEV). However, their mechanism is not well understood. The flow visualization technique is a promising method to illustrate the complex flow field spatially and temporally without any intrusion. A basic flow visualization setup consists of a high power laser and optic lenses to generate the laser sheet, a camera, a tracer particle generator and a data processer. The practical setup, specifications of devices involved and the corresponding parameter settings are dependent on the flow features to be obtained.

The normal smoke wire flow visualization uses a smoke wire to demonstrate the flow streaklines. However, the performance of this method is limited by poor spatial resolution when conducting in a complex flow field. Therefore, a smoke flow visualization similar with the particle image velocimetry (PIV) measurement is developed. This method can illustrate the large-scale global LEV flow field and the small-scale shear layer flow structure at the same time, providing a valuable reference for the later detailed PIV measurement.

A detailed description for applying the flow visualization methods to study the unsteady flow phenomena over a delta wing is presented in this paper. The procedure and cautions to conduct the experiment are listed, including wind tunnel setup, parameters adjusting and data processing. The representative results demonstrate that the flow visualization methods are effective techniques for investigating the three-dimensional flow field qualitatively and quantitatively.

INTRODUCTION:

The flow field measurement via visualization techniques is the one of the basic methodologies in the fluid engineering to acquire the flow features. Among different visualization techniques, the smoke wire flow visualization in the wind tunnel experiments and the dye visualization in the

water tunnel experiments are the most widely used techniques to illustrate the flow structures qualitatively. On the other hand, the particle image velocimetry (PIV) and the laser Doppler anemometry (LDA) are two typical quantitative techniques[1].

For the smoke wire flow visualization, smoke streaklines are generated from oil droplets on a heating wire or injected from the outer smoke generator/container during the experiments. High power lights or laser sheets are used to illuminate the smoke streaklines. Images are then recorded for further analyses. It is a simple but very useful means of flow visualization method[2]. However, the effectiveness of this method may be limited by a few factors, such as the short duration of smoke with good quality, the complex three-dimensional flow field, the relatively high velocity of the flow and the efficiency of smoke generating[3].

In the PIV measurements, a cross section in the flow field is illuminated by two separated laser sheets at a very small time interval and recorded by a high-speed camera as a pair of images. By dividing the images into a grid of interrogation areas and calculating the average motion of particles in interrogation areas through cross-correlation functions, the instantaneous velocity vector map in this observed cross section can be obtained. However, it is also known that a few compromises need to be reached among the factors of the size of the observation window, the resolution of the velocity map, the velocity magnitude in the plane, the time interval between the pair of images, the orthogonal velocity magnitude and the particle density[4]. Therefore, a lot of exploratory experiments might be needed to optimize the experimental settings. It would be expensive and time-consuming if one investigates an unknown and complex flow field only with the PIV measurement[5,6]. Considering the above concerns, a strategy to combine the smoke flow visualization and the PIV measurement is proposed and demonstrated to study the complex flow over a slender delta wing.

As known, numerous studies on LEV flows over delta wings were reported[7,8] in the past decades, with flow visualization techniques as the major tools. Many interesting flow phenomena were observed, such as, the spiral type and bubble type vortex breakdowns[9,10], the unsteady shear layer substructure[11,12], oscillations of LEV breakdown locations[13], and effects of pitching and yaw angles[14-16] on the flow structures. Nevertheless, the underlying mechanisms of some unsteady phenomena in the delta wing flows are still unclear[7]. In this work, the smoke flow visualization is improved by using the same seeding particles as in the PIV measurement, instead of the smoke wire. This improvement greatly simplifies the operation of the visualization and increases the quality of the images. Based on the results from the improved smoke flow visualization, the PIV measurement focuses on those interesting flow fields to acquire the quantitative information.
Here, a detailed description is provided to explain how to conduct the flow visualization experiment in the wind tunnel and investigate the unsteady flow phenomena over a delta wing. Two visualization methods are used together in this experiment, the improved smoke flow visualization and the PIV measurement. The procedure includes the step-by-step guidance for devices setup and parameters adjustment. Typical results are demonstrated to show the advantage of combining these two methods for measuring the complex flow field spatially and temporally.

PROTOCOL:

1. Wind Tunnel Setup

The experiments are conducted in a closed-loop low speed wind tunnel in The Hong Kong Polytechnic University. The test section is 2.4 m (length) × 0.6 m (width) × 0.6 m (height). The test section is equipped with glass walls that allow optical access during the experiments. The turbulent intensity of this facility is less than 0.4 %. In this study, the freestream velocity U_∞ ranges from 2.64 $m\ s^{-1}$ to 10.56 $m\ s^{-1}$, corresponding to Reynolds number, Re, from 5×10^4 to 2×10^5 based on the chord length of the delta wing, which is the typical flight range for an unmanned aerial vehicle (UAV). The delta wing model used in this study is made of aluminum, with the swept angle φ = 75°, the chord length c = 280 mm, the root span b = 150 mm and the thickness 5 mm. Both leading edges are beveled at 35° to fix the separation point[17] (see Figure 1(a)). Figures 1(b) and 1(c) show the schematics of the wind tunnel setup and the arrangements of the laser sheet and cameras for observation in different cross sections, respectively. Note that the setup of Figure 1(b) is detailed as follows.

1.1. Install the delta wing.

1.1.1. Fix the delta wing trailing edge on the sting, which is on a circular motion guide used for adjusting the angle of attack (AoA). The center of the circular guide is on the central line of the wind tunnel test section (see in **Figure 1(b)**). Thus, the delta wing center can always be at the center of the test section. Adjust the AoA to 34°.

1.1.2. Carefully adjust the delta wing model to minimize any yaw angle and roll angle, by checking the readings of an angle meter and a three-axis laser level. In the current study, the uncertainty of these two angles is less than 0.1 °.

1.2. Set up the laser sheet.

1.2.1. Two lasers are used separately to illuminate the flow structures for the PIV measurement and the smoke flow visualization, respectively. The one used in the PIV measurement is a dual pulse laser, with the wavelength of 532 nm and maximum energy of 600 mJ (adjustable) for each pulse. Another one used in the smoke flow visualization is a continuous laser with the wavelength of 532 nm and the power of 1 W. During the setup installation, the laser beam is filtered by a neutral density filter with 10% transmittance, for the safety concern.

1.2.2. Install laser optics to form the laser sheet. The convex lens is used to control the laser beam size (also the sheet thickness). The cylindrical lens expands the laser beam to a laser sheet. The expansion angle of the laser sheet is determined by the diameter of the cylindrical lens. In the current study, the focal length of the cylindrical lens is 700 mm, the diameter of the cylindrical lens is 12 mm.

1.2.3. Adjust the reflection mirror to introduce the laser sheet into the wind tunnel. In the spanwise cross section cases (see in Figure 1(c)), the angle between the laser light axis and the

mirror is $\frac{1}{2}(90° - \alpha)$, where α is the angle of attack. According to the result of spanwise measurement, the spatial position of LEVs can be obtained. Thus, the laser sheet positions in the transverse and longitudinal cross sections is determined. In the longitudinal cross section cases, the angle between the laser light axis and the mirror is 45°. In the transverse cross section cases, the angle between the laser light axis and the mirror is also dependent on the angle of attack, which determines the spatial positions of LEV cores. For example, in the case with $\alpha = 44°$, the angle between the laser light axis and the mirror is $71°$. Make sure that the central of the laser sheet (the dominant energy of the laser) is in the field of view (FOV).

1.2.4. Check the laser sheet thickness by measuring the laser line on the model. Adjust the location of the convex lens if the laser sheet thickness is not suitable. Determine the thickness according to the velocity component in the vertical direction relative to the laser sheet plan. Otherwise it will cause problem in the PIV data processing because most of the particles in the first frame may move out of the second frame. In this experiment, the thickness of the laser sheet is around 1 mm, and the effective width of the laser sheet in the test section is about 100 mm.

1.2.5. Put a target plate on the delta wing, with its surface coincident to the FOV[18]. Modify the laser sheet position until it is coincident to this target plate, by rotating the cylindrical lens and the reflection mirror. This step is important since the FOV in the current study is not orthogonal to the wind tunnel coordinate.

1.3. Camera setup.

1.3.1. Turn off the lasers when setting up the camera. Two cameras are involved in this experiment. One is a high-speed CCD camera with a resolution of 2048 × 2048 pixels for the PIV measurement. The other one is a commercial digital camera with a snapshot resolution of 4000 × 6000 pixels and a 50 Hz videoing resolution of 720 × 1280 pixels during the smoke flow visualization.

1.3.2. Move the camera position to have the proper FOV as desired. Adjust the camera lens to focus on the target plate. During this step, make sure that entire field is focused. If not, it indicates that the coordinate of the camera is not orthogonal to the target plate. Thus, adjust the camera position carefully.

1.3.3. Take several frames after the camera is well set. Later, these frames of the target plate are used to calibrate the scale factor between the real size and the frame pixel.

1.4. Turn on the wind tunnel at a low speed (for example, 3 m/s) and inject oil particles into the wind tunnel. In this pre-seeded flow visualization method, the whole wind tunnel is uniformly seeded with olive oil particles produced by an aerosol generator. The diameter of injected particles is about 1 μm. Typically, it takes about 30 seconds to inject oil particles of 1.5 grams into the wind tunnel. During the experiment, the oil particle density concentration in the wind tunnel is approximately $650\ \mu g/m^3$, thus the overall flow density change $\frac{\rho' - \rho}{\rho} < 0.1\%$.

1.5. PIV software setup

1.5.1. The PIV system is controlled by the imaging software (see **Table of Materials**). This software can command the synchronizer to send transistor-transistor logic (TTL) signals to the laser and the camera.

1.5.2. Set the sampling frequency at 5 Hz, with a total sampling number of 500. The time interval between PIV frames is 80 μs. Note that the time interval is dependent on the size of the FOV and flow velocity. Make sure that the interrogation areas in two frames have about 50% ~ 75% overlap.

2. Running the Experiment

2.1. The improved smoke flow visualization

2.1.1. Turn on the wind tunnel at the desired freestream velocity. Run it for 10 minutes to uniform the freestream velocity and temperature. At Re = 50,000, the freestream velocity is U = 2.64 m/s.

2.1.2. Turn on the continuous laser. Use the digital camera to capture $5-10$ snapshots of the flow structure.

2.1.3. Check whether the laser sheet is at the axial cross section of the LEV core. If yes, mark this position on the delta wing model as a reference for the later PIV measurement; otherwise, adjust the optic lens following steps 1.2.2-1.2.5.

2.1.4. Review those images and check the focusing and the brightness. If the image quality is not satisfactory, adjust the camera lens or the ISO setup, correspondingly.

2.1.5. Take more snapshots (typically around 20) and videos (around 40 seconds) with the proper setup. Turn off the laser and transfer the data to the computer.

2.2. PIV measurement

2.2.1. Based on the reference position known from step 2.1.3 and the results from the improved smoke flow visualization, choose an interesting region ($x/c \approx 0.3$) where vortical substructures can be observed and adjust the setup.

2.2.2. Turn on the wind tunnel at the desired freestream velocity, $U = 2.64$ m/s. Run it for 10 minutes to uniform the freestream velocity distribution and temperature.

2.2.3. Adjust the dual pulse laser to the highest power level and standby. Wear the laser-protection goggles properly. Use the software to start the data acquisition for 100 seconds.

2.2.4. Once the data recording is finished, make the laser offline. Review the acquired images in the software and check the laser sheet distribution, the particle density (6 - 10 particles in each interrogation area), the focusing and particle displacement between the double frames (25% - 50% of the interrogation area).

2.2.5. If the quality of images is satisfied, save the data into the hard disk of the PC and run the other cases by repeating the above steps. Otherwise, repeat steps 1.2.4 - 1.5.2 to adjust the setup carefully and then follows steps 2.2.1-2.2.4.

3. Data Processing

3.1. The improved smoke visualization

3.1.1. Transform the video into a sequence of frames. Convert the frames from the RGB form into the gray scale. Rotate the frame to make the delta wing surface horizontal. Choose the area of interesting for later processing. (**Figure 2(a)**)

3.1.2. Adjust the brightness and the contract to highlight the flow structure. Apply an adaptive threshold to transfer the gray image into a binary image. (**Figure 2(b)**)

3.1.3. Add up the binary value in each column and find the position at which the sum suddenly changes. This position is determined as the vortex breakdown location (**Figure 2(c)**).

3.1.4. Step 3.1.1-3.1.3 can be done automatically (see the supplemental coding file). Record all the vortex breakdown locations and their corresponding time. Thus, the time history of the breakdown oscillation can be obtained.

3.1.5. Use the images with the target plate to scale the real positions. Plot the time history of the breakdown oscillation.

3.2. PIV measurement

3.2.1. The PIV analysis is also performed with the imaging software. Use the images acquired in step 1.3.3 to set the scale factor and the reference position of the coordinate. Pre-process the acquired data through image processing library to highlight the particles and reduce the noise[18].

3.2.2. An adaptive interrogation area method is used, with the minimum grid size of 32 × 32 pixels and the minimum overlap of 50 %. Choose the image area and set 3×3 vector validation for the adaptive cross-correlations.

3.2.3. The result comes out as a velocity vector field, in which the blue vectors are the correct vectors, the green ones are the substituted vectors, and the red ones are bad ones.

3.2.4. Apply the 3×3 moving average validation method to estimate the true local velocity by comparing the vectors in its neighborhood. Vectors that deviate too much from their neighbors are replaced by the average of the neighbors.

3.2.5. Calculate vector statistics in the velocity maps to obtain the flow characteristics in the time history, such as the time-averaged velocity, the standard deviation and the cross correlation between velocity components. Compute the scalar derivatives from the vector map to demonstrate the internal features of the flow field, such as the vorticity, shear stresses and the swirling strength.

REPRESENTATIVE RESULTS:

Figure 2(d) shows the time histories of the LEV breakdown locations. The black one is for the portside LEV and the red one is for the starboard LEV. The time scale is nondimensionalized by the free stream velocity and the chord length. The correlation coefficient between these two time histories is $r = -0.53$, indicating a strong anti-symmetric interaction of the LEV breakdown location oscillations. This result well agrees with others work[13,19,20].

Figure 3 shows the LEV flow structure in the streamwise cross section at $\alpha = 44°$ and $Re = 75{,}000$. The original image was captured by the digital camera in the RGB form, with an exposure duration of 1/500 second. In this figure, the coordinate is normalized by the delta wing chord length. A 10 mm scale is plotted at the upper right corner for reference. The result clearly demonstrates the primary LEV core, which develops from the tip of the delta wing to the downstream in a straight line. Near the position at $x = 0.19c$, the vortex core suddenly expands. This is known as the leading edge vortex breakdown[9,21]. After the breakdown location, the wake becomes turbulent. Around the primary LEV core, there are small vortical structures. These substructures originate from the leading edges and swirl around the primary vortex core within the rolling up shear layer[12,22,23]. As the substructures move into the inner layer of the LEV, their shape is stretched due to the relatively high velocity component in the streamwise direction near the vortex core. During the experiment, it is noted that the flow structure of the LEV is quite stationary except the LEV breakdown location. This result shows that this smoke flow visualization method can achieve a good balance between the local small flow structure and the global flow structure evolution.

Figure 4 shows the typical particle images in a 64×64 pixels region, captured from the PIV measurement. In the 32×32 pixels interrogation area in Frame A, there are 10 identified particles, marked by yellow circles. After the time interval between two frames, these particles displace to new locations, as shown in Frame B. The displacements are about one-quarter of the interrogation area, resulting to an almost 70 % overlap between these interrogation areas. Additionally, almost all the particles remain in the laser sheet plane, indicating that the setup parameters are properly chosen for this case.

Figure 5 shows the time-averaged PIV results in the streamwise and spanwise cross sections. To get this result, the improved smoke flow visualization is conducted firstly to identify the primary vortex core position, following steps 2.1.1-2.1.3. The coordinates in **Figure 5** are normalized by

the delta wing chord length and the local semispan length, respectively. The vorticity contour is normalized as $\omega^* = \omega U_\infty / c$. According to this result, the primary vortex core can be easily identified by the inflection line of the positive and negative vorticities, and is marked by the black dot line. In the upper and bottom regions, the rolling shear layers show large vorticities. The λ_{ci} criterion[24,25] is used to identify the vortices from the PIV measurement. In **Figure 5**, the solid lines illustrate the region with the local swirling strength lower than zero, indicating the existence of vortices. Near the core, the substructures are stretched and do not appear in the swirling strength contour. However, the concentrated vorticity contour still suggests the substructures here, marked by the white dot line. In **Figure 5(b)**, the velocity vector map clearly illustrates that on each side, the flow separates at the leading edge and forms a strong shear layer, which later rolls into the LEV core. Complementary to the flow structure in the streamwise cross section, the spanwise flow structure clearly shows the evolution of the outer vortical substructures.

FIGURE AND TABLE LEGENDS:

Figure 1. Schematics of setups. (a) the delta wing model, (b) the wind tunnel setup, and (c) setups of the laser sheet and camera for observation in different cross sections.

Figure 2. (a) A smoke flow visualization result showing the leading edge vortex structure in the transverse cross section: $\boldsymbol{\alpha}$=$\mathbf{44}$°; $\boldsymbol{Re}$=$\mathbf{50{,}000}$. (b) The processed binary image of the LEV breakdown. (c) The summation of each column in the binary image (Fig. 2(b)) and the identified LEV breakdown location in the streamwise direction (x-direction). (d) The time histories of the LEV breakdown locations.

Figure 3. The leading edge vortex structure in the streamwise cross section at $\boldsymbol{\alpha = 44°}$ and $\boldsymbol{Re = 75,000}$, obtained from the smoke flow visualization.

Figure 4. Particle images in a $\mathbf{64 \times 64}$ pixels region. The corresponding interrogation area is 32×32 pixels. The time interval between Frame A and B is 80 microseconds. The identified particles in the original interrogation area are marked by yellow circles.

Figure 5. Time-averaged PIV results. (a) Vorticity contour with solid lines marking the regions with the local swirling strength lower than zero in the streamwise cross section. (b) Vorticity contour with velocity vectors in the spanwise cross section at $x = 0.4c$. ($\boldsymbol{\alpha}$=$\mathbf{34}$° and $\boldsymbol{Re}$=$\mathbf{50{,}000}$)

DISCUSSION:

This article presents the two flow visualization methods, the improved the smoke flow visualization and the PIV measurement, to investigate the flow structure over the delta wing qualitatively and quantitatively. The general procedures of the experiment are described step by step. The setup of these two methods are almost the same while the devices involved are different. The basic principle of these two flow visualization methods is to use the laser sheet to illuminate the particles in the flow. The improved smoke flow visualization can obtain the global flow structure and the local small structures at the same time, which is helpful to get an overview of the unknown flow structure. The quantitative PIV analysis provides a detailed vector map of

the interesting flowfield. Therefore, the combination of these flow visualization methods can greatly improve the research efficiency.

Compared with the normal smoke wire flow visualization, the smoke flow visualization method demonstrated here is rather easily conducted. Because the particles are uniformly distributed, small flow structures are easily identified. In a complex three-dimensional flow, this method allows the laser sheet to be set up at any spatial position to observe the flow fields in difference cross sections, whereas in the traditional smoke wire method, the laser sheet needs always to be aligned with the smoke direction and the observation window is limited accordingly[26]. Additionally, this improved method will not miss any flow details caused by the absence of the smoke in some regions during the smoke wire experiment. However, this method will not be suitable for open-loop wind tunnel facilities due to the seeding problem. Also, flow visualization data should be carefully analyzed to avoid pitfalls of imaginary illuminations[3,27].

Because the flow field over the delta wing is highly three-dimensional and it is sensitive to any disturbance, non-intrusive investigations are recommended[21]. For measurements in planes, it is very important to consider the orthogonal velocity component on the observation plane during the PIV measurement[28,29]. In this case, the time interval between two frames and the laser sheet thickness should be compromised with the orthogonal velocity, to ensure that most of the particles would not move out the laser sheet. For similar measurement, it is suggested to run several cases with different setup parameters in advance to find out the suitable ones.

The flow visualization methods described in this paper are convenient, effective and low-cost. In the future, these techniques will be applied to complex flow fields with active flow control, such as bluff body drag reduction and vortex-structure interaction, in order to evaluate the control effect quickly, understand the control mechanism and accelerate the optimization of control parameters.

ACKNOWLEDGMENTS:

The authors would like to thank Hong Kong Research Grants Council (no. GRF526913), Hong Kong Innovation and Technology Commission (no. ITS/334/15FP), and the US Office of Naval Research Global (no. N00014-16-1-2161) for financial support.

DISCLOSURES:

The authors have nothing to disclose.

REFERENCES:

1 Smits, A. J. *Flow visualization: techniques and examples*. (World Scientific, 2012).

2 Barlow, J. B., Rae, W. H. & Pope, A. *Low-Speed Wind Tunnel Testing*. (New York: Wiley, 1999).

3 Merzkirch, W. *Flow visualization*. (Academic Press, inc, 1987).

4 Raffel, M., Willert, C. E., Wereley, S. & Kompenhans, J. *Particle image velocimetry: a practical guide*. (Springer, 2007).

5 Westerweel, J., Elsinga, G. E. & Adrian, R. J. Particle Image Velocimetry for Complex and

Turbulent Flows. *Annu Rev Fluid Mech.* **45** (1), 409-436, doi:10.1146/annurev-fluid-120710-101204, (2013).
6 Meinhart, C. D., Wereley, S. T. & Santiago, J. G. PIV measurements of a microchannel flow. *Exp. Fluids.* **27** (5), 414-419, doi:10.1007/s003480050366, (1999).
7 Gursul, I. Review of Unsteady Vortex Flows over Slender Delta Wings. *J AIRCRAFT.* **42** (2), 299-319, doi:10.2514/1.5269, (2005).
8 Gursul, I., Gordnier, R. & Visbal, M. Unsteady aerodynamics of nonslender delta wings. *PROG AEROSP SCI.* **41** (7), 515-557, doi:10.1016/j.paerosci.2005.09.002, (2005).
9 Lowson, M. Some experiments with vortex breakdown(Water tunnel flow visualization on slender delta wings reveal vortex breakdown formation to be a nonaxisymmetric stability). *ROYAL AERONAUTICAL SOCIETY JOURNAL.* **68** 343-346 (1964).
10 Payne, F. M., Ng, T., Nelson, R. C. & Schiff, L. B. Visualization and wake surveys of vortical flow over a delta wing. *AIAA J.* **26** (2), 137-143, doi:10.2514/3.9864, (1988).
11 Lowson, M. V. The three dimensional vortex sheet structure on delta wings. *Fluid Dynamics of Three-Dimensional Turbulent Shear Flows and Transition.* 11.11-11.16 (1989).
12 Riley, A. J. & Lowson, M. V. Development of a three-dimensional free shear layer. *J. Fluid Mech.* **369** 49-89 (1998).
13 Menke, M. & Gursul, I. Unsteady nature of leading edge vortices. *Phys. Fluids.* **9** (10), 2960, doi:10.1063/1.869407, (1997).
14 Yayla, S., Canpolat, C., Sahin, B. & Akilli, H. Yaw angle effect on flow structure over the nonslender diamond wing. *AIAA J.* **48** (10), 2457-2461 (2010).
15 Menke, M. & Gursul, I. Nonlinear Response of Vortex Breakdown over a Pitching Delta Wing. *J AIRCRAFT.* **36** (3), 496-500, doi:10.2514/2.2481, (1999).
16 Sahin, B., Yayla, S., Canpolat, C. & Akilli, H. Flow structure over the yawed nonslender diamond wing. *AEROSP SCI TECHNOL.* **23** (1), 108-119 (2012).
17 Kohlman, D. L. & Wentz, J. W. H. Vortex breakdown on slender sharp-edged wings. *J AIRCRAFT.* **8** (3), 156-161, doi:10.2514/3.44247, (1971).
18 Lu, L. & Sick, V. High-speed Particle Image Velocimetry Near Surfaces. *JoVE.* (76), 50559, doi:10.3791/50559, (2013).
19 Mitchell, A. M., Barberis, D., Molton, P., Dé, J. & lery. Oscillation of Vortex Breakdown Location and Blowing Control of Time-Averaged Location. *AIAA J.* **38** (5), 793-803, doi:10.2514/2.1059, (2000).
20 Shen, L., Wen, C.-y. & Chen, H.-A. Asymmetric Flow Control on a Delta Wing with Dielectric Barrier Discharge Actuators. *AIAA J.* **54** (2), 652-658, doi:10.2514/1.j054373, (2016).
21 Leibovich, S. The Structure of Vortex Breakdown. *ANNU REV FLUID MECH.* **10** (1), 221-246, doi:10.1146/annurev.fl.10.010178.001253, (1978).
22 Mitchell, A. M. & Molton, P. Vortical Substructures in the Shear Layers Forming Leading-Edge Vortices. *AIAA J.* **40** (8), 1689-1692, doi:10.2514/2.1844, (2002).
23 Gad-El-Hak, M. & Blackwelder, R. F. The discrete vortices from a delta wing. *AIAA J.* **23** (6), 961-962, doi:10.2514/3.9016, (1985).
24 Zhou, J., Adrian, R. J., Balachandar, S. & Kendall, T. M. Mechanisms for generating coherent packets of hairpin vortices in channel flow. *J. Fluid Mech.* **387** 353-396, doi:10.1017/s002211209900467x, (1999).
25 Adrian, R. J., Christensen, K. T. & Liu, Z. C. Analysis and interpretation of instantaneous

turbulent velocity fields. *Exp. Fluids.* **29** (3), 275-290, doi:10.1007/s003489900087, (2000).
26 Yoda, M. & Hesselink, L. A three-dimensional visualization technique applied to flow around a delta wing. *Exp. Fluids.* **10-10** (2-3), doi:10.1007/bf00215017, (1990).
27 Greenwell, D. I. in *RTO AVT Symposium* RTO-MP-069(I) (Loen, Norway, 2001).
28 Furman, A. & Breitsamter, C. Turbulent and unsteady flow characteristics of delta wing vortex systems. *AEROSP SCI TECHNOL.* **24** (1), 32-44, doi:10.1016/j.ast.2012.08.007, (2013).
29 Wang, C., Gao, Q., Wei, R., Li, T. & Wang, J. 3D flow visualization and tomographic particle image velocimetry for vortex breakdown over a non-slender delta wing. *Exp. Fluids.* **57** (6), doi:10.1007/s00348-016-2184-y, (2016).

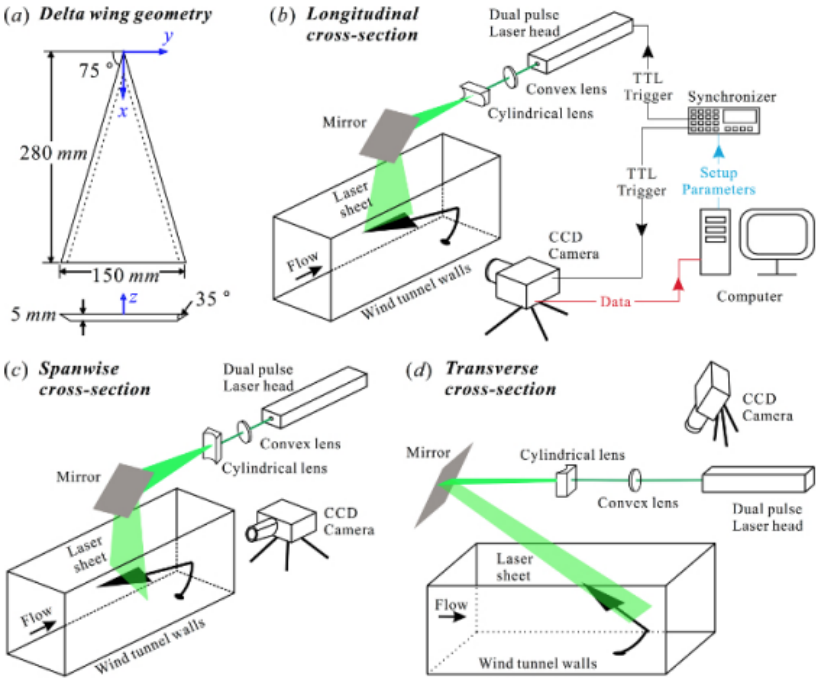

Figure 1: Schematics of setups. (a) The delta wing model; **(b-d)** setups for PIV measurement in the longitudinal cross-section, the spanwise cross-section, and the transverse cross-section, respectively. Please click here to view a larger version of this figure.

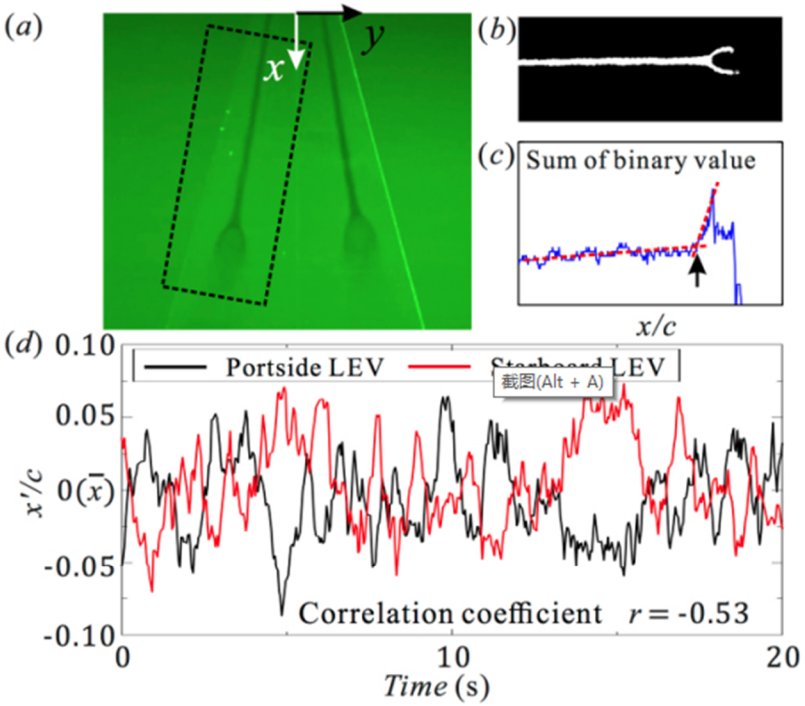

Figure 2: Measurement of the LEV breakdown location. (a) A smoke flow visualization result showing the leading-edge vortex structure in the transverse cross section: α = 34° and *Re* = 50,000; the marked area is rotated and further processed. **(b)** The binary image of the marked area in (a), clearly showing the LEV core and breakdown. **(c)** The summation of each column in the binary image (b) and the identified LEV breakdown location in the streamwise direction (x-direction), normalized by the chord length *c*. **(d)** The time histories of the LEV breakdown locations. $\bar{x}$ is the time-averaged position and x' is the instant distance to the time-averaged position. Please click here to view a larger version of this figure.

454

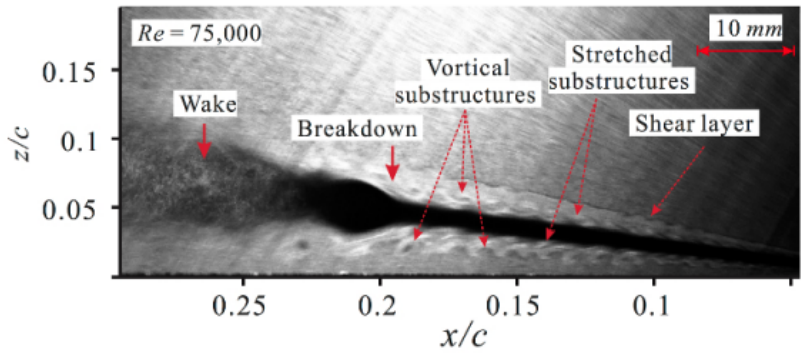

Figure 3: The leading-edge vortex structure in the longitudinal cross section at α = 34° and *Re* = 75,000, obtained from the smoke flow visualization. Please click here to view a larger version of this figure.

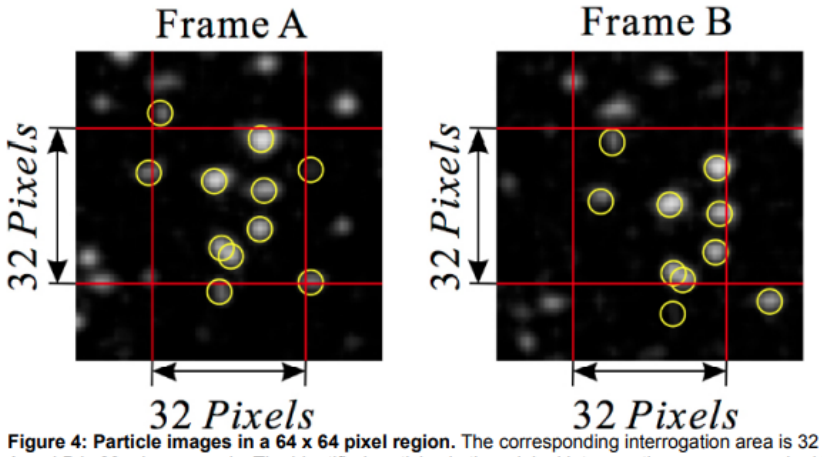

Figure 4: Particle images in a 64 x 64 pixel region. The corresponding interrogation area is 32 x 32 pixels. The time interval between Frames A and B is 80 microseconds. The identified particles in the original interrogation area are marked by yellow circles. Please click here to view a larger version of this figure.

455

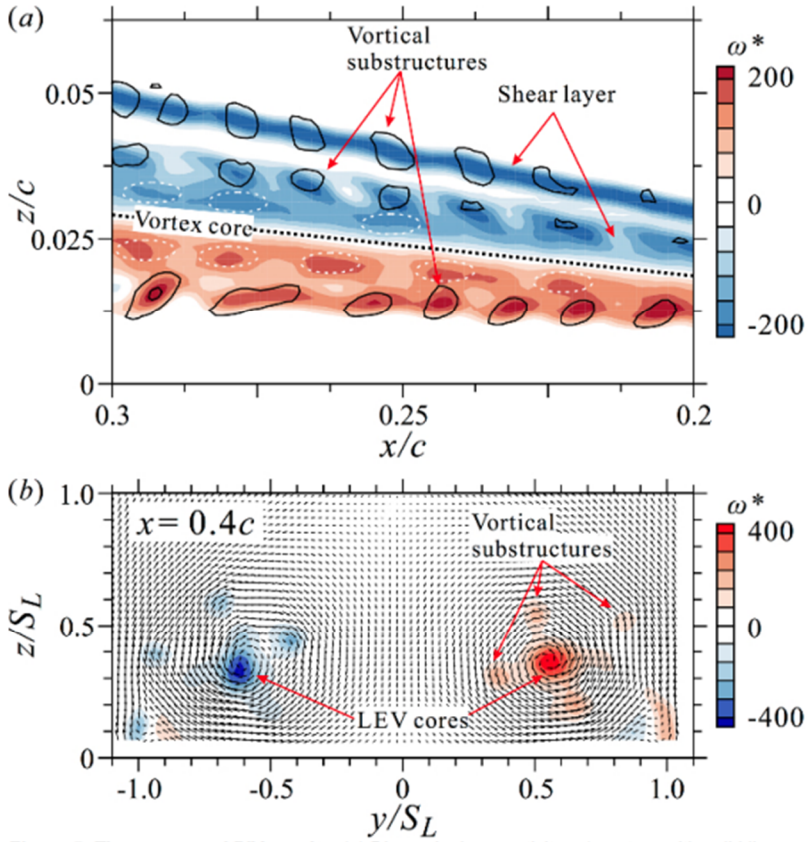

Figure 5: Time-averaged PIV results. (**a**) Dimensionless vorticity ω^* contour with solid lines marking the regions with local swirling strength lower than zero in the longitudinal cross section. (**b**) Dimensionless vorticity ω^* contour with velocity vectors in the spanwise cross section at x = 0.4c; coordinates are normalized by the local semispan length S_L (α = 34° and Re = 50,000). Please click here to view a larger version of this figure.

456